Journal of Atmospheric and Solar-Terrestrial Physics 174 (2018) 46–65

Contents lists available at ScienceDirect

Journal of Atmospheric and Solar-Terrestrial Physics

journal homepage: www.elsevier.com/locate/jastp

Multi-instrument view on solar eruptive events observed with the Siberian Radioheliograph: From detection of small jets up to development of a shock wave and CME

V.V. Grechnev, S.V. Lesovoi*, A.A. Kochanov, A.M. Uralov, A.T. Altyntsev, A.V. Gubin, D.A. Zhdanov, E.F. Ivanov, G.Ya. Smolkov, L.K. Kashapova

Institute of Solar-Terrestrial Physics, Irkutsk, Russia

A R T I C L E I N F O

Keywords:
Coronal mass ejections
Instrumentation and data management
Prominences
Radio bursts
Surges
Shock waves

A B S T R A C T

The first 48-antenna stage of the Siberian Radioheliograph (SRH) started single-frequency test observations early in 2016, and since August 2016 it routinely observes the Sun at several frequencies in the 4–8 GHz range with an angular resolution of 1–2 arc minutes and an imaging interval of about 12 s. With limited opportunities of the incomplete antenna configuration, a high sensitivity of about 100 Jy allows the SRH to contribute to the studies of eruptive phenomena along three lines. First, some eruptions are directly visible in SRH images. Second, some small eruptions are detectable even without a detailed imaging information from microwave depressions caused by screening the background emission by cool erupted plasma. Third, SRH observations reveal new aspects of some events to be studied with different instruments. We focus on an eruptive C2.2 flare on 16 March 2016 around 06:40, one of the first flares observed by the SRH. Proceeding from SRH observations, we analyze this event using extreme-ultraviolet, hard X-ray, white-light, and metric radio data. An eruptive prominence expanded, brightened, and twisted, which indicates a time-extended process of the flux-rope formation together with the development of a large coronal mass ejection (CME). The observations rule out a passive role of the prominence in the CME formation. The abrupt prominence eruption impulsively excited a blast-wave-like shock, which appeared during the microwave burst and was manifested in an “EUV wave” and Type II radio burst. The shock wave decayed and did not transform into a bow shock because of the low speed of the CME. Nevertheless, this event produced a clear proton enhancement near Earth. Comparison with our previous studies of several events confirms that the impulsive-piston shock-excitation scenario is typical of various events.

1. Introduction

Solar flares, coronal mass ejections (CMEs), associated shock waves, and related phenomena are known as causes of space weather disturbances. Hard electromagnetic emissions and energetic particles pose hazard to space-borne equipment, astronauts on spacecraft, and even crew members and passengers on aircraft that carry out transocean flights entering high latitudes. CME-associated shock waves travel over large distances in the heliosphere, being responsible for the geomagnetic storm sudden commencement (SSC). Magnetic structures of CMEs hitting the Earth’s magnetosphere can cause strong geomagnetic storms.

In spite of a certain space weather impact, the origin and interrelation of solar eruptive phenomena are still not quite clear. Comprehending solar eruptions is hampered by observational difficulties. The existing concepts are mostly based on the hypotheses that were proposed several decades ago and back-extrapolated results of in-situ measurements in near-Earth space.

According to a widely accepted view, the main driver of a solar eruption is a magnetic flux rope. It is considered as the active structure of a CME that governs its development and subsequent expansion. The flux rope is traditionally assumed to be associated with the CME cavity. Prominences (filaments) or associated structures appear to be among the most probable flux-rope progenitors (Gibson, 2015). However, genesis of flux ropes, their size range, and other properties are not clear so far. According to some concepts, the flux rope pre-exists before the eruption onset (Chen, 1989, 1996; Cheng et al., 2013). Different concepts relate the flux-rope formation to reconnection processes, which are also responsible for solar flares (Inhester et al., 1992; Longcope and Beveridge, 2007; Qiu et al., 2007).

There is no consensus about coronal shock waves. Some authors advocate flare-ignited blast waves at least in some events (Magdalenić

* Corresponding author.
E-mail address: svlesovoi@gmail.com (S.V. Lesovoi).

https://doi.org/10.1016/j.jastp.2018.04.014
Received 25 January 2018; Received in revised form 24 April 2018; Accepted 26 April 2018
Available online 03 May 2018
1364-6826/

et al., 2010, 2012; Nindos et al., 2011). Different studies demonstrate the CME-related origin of shock waves to be more probable (e.g. Cliver et al., 2004). While basic excitation mechanisms of shock waves seem to be known (see, e.g., Vršnak and Cliver, 2008), observational difficulties result in large uncertainties in their identification.

Solar eruptions and associated phenomena are manifested in different spectral domains, including microwaves. Radio emission is produced by various mechanisms, providing important information on these phenomena and responsible processes. Being sensitive to gyrosynchrotron emission of nonthermal electrons, microwaves reveal the flare regions. The microwave spectrum contains information about accelerated electrons and magnetic fields in the corona. Being sensitive to thermal plasma emission, microwave images show eruptive prominences (filaments). Screening background solar emission by erupted prominence material sometimes produces depressions detectable even in the total microwave flux (Covington and Dodson, 1953) termed the "negative bursts". From studies of the negative bursts, events with reconnection between erupting structures and a large-scale coronal magnetic environment were identified (Grechnev et al., 2013b, 2014b; Uralov et al., 2014). These examples demonstrate significant contribution to studies of solar eruptions from microwave imaging and non-imaging observations.

Microwave images produced by radio heliographs generally have a poorer spatial resolution relative to extreme-ultraviolet (EUV) and X-ray telescopes. Nevertheless, sometimes it is even possible to judge about the structures that are unresolved in microwave images (Grechnev and Kochanov, 2016; Grechnev et al., 2017a; Lesovoi et al., 2017).

In 2016, the first 48-antenna stage of the Siberian Radioheliograph (SRH; Lesovoi et al., 2014, 2017) started observing the Sun. An overview of the SRH data has revealed several indications of eruptions. Proceeding from these indications, we consider a few eruptive events observed by different instruments and endeavor to address the challenges listed in this section. We pay special attention to the 16 March 2016 eruptive event, one of the first flares observed by the SRH (Lesovoi et al., 2017). Multi-instrument analysis of large-scale aspects of this event promises shedding additional light on the development of a CME and associated shock wave.

Section 2 outlines the SRH. Section 3 presents observations of microwave depressions caused by small jets. Section 4 presents direct observations of a spray on 1 May 2017. Section 5 is devoted to a multi-instrument analysis of an eruptive event on 16 March 2016 that produced a CME and caused a near-Earth proton enhancement. Section 6 discusses the results and shows their relevance to a typical eruptive event. Section 7 summarizes our conclusions and their implications and presents last changes in the functionality of the SRH.

2. SRH: 48-antenna first stage

The SRH was constructed as an upgrade of the Siberian Solar Radio Telescope (SSRT: Smolkov et al., 1986; Grechnev et al., 2003). The SSRT was designed as a cross-shaped interferometer comprising two linear arrays in the EW and SN directions, each with 128 equidistant antennas of 2.5 m diameter spaced by $d = 4.9$ m. The SSRT scans the Sun due to its diurnal passage through the fan beam formed by the simultaneous receiving at a number of different but close frequencies in the 5.67–5.79 GHz band. Thus, the SSRT can produce the images practically at a single frequency every 2–3 min at most.

Unlike the directly-imaging SSRT, the SRH uses the Fourier synthesis. The temporal resolution determined by the receiver system is much higher than the SSRT had. The SRH has a T-shaped antenna array. Its 1.8 m antenna elements replace old SSRT antennas, being installed at the existing posts along the east, west, and south arms. The first 48-antenna stage constitutes a dense equidistant part of a future complete SRH antenna array (Figs. 1 and 2). Being redundant, this array provides a high sensitivity, which is about 1000 K in the images and reaches for compact sources 10^{-4} of the total solar flux, i.e. about 100 Jy (Lesovoi and Kobets, 2017).

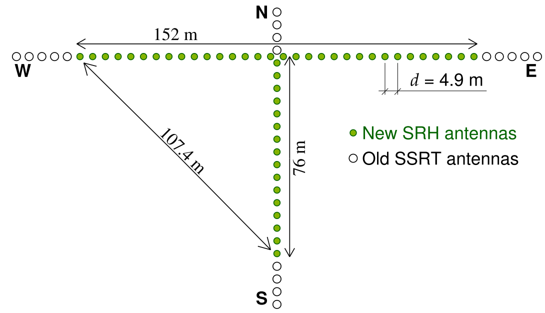

Fig. 1. The T-shaped configuration of the 48-antenna SRH first stage. The remote parts of the four SSRT arms (each arm of 311 m) with remaining old antennas are not shown.

Both circularly-polarized components are measured. The observing frequencies, each of the 10 MHz bandwidth in the 4–8 GHz range, are set by software and can be optimized for an observing program. The accumulation time at each frequency is 0.28 s for each circularly-polarized component, and the time to switch from one frequency to another was about 2 s in 2016 and 2017. The maximum baseline used is 107.4 m, enabling a spatial resolution down to 70″ at 8 GHz.

The SRH systems outlined in Fig. 3 were mostly developed and constructed by the SRH team. The top image represents a single antenna element. The antenna feed receives two orthogonal linearly-polarized signals, which come into the frontend unit. A 3-dB 90° hybrid coupler performs the linear-to-circular polarization conversion of the input signals. Then they are pre-amplified and come to a switch, which alternately passes the left-handedly polarized signal (LCP) and the right-handedly polarized one (RCP). The signals from the output of the switch come through the second amplifier to a diode laser, which converts the ultrahigh-frequency (UHF) signals to optical signals for their transmission to the working building. The total gain of the frontend unit is 30–40 dB.

The signal from each antenna element is transmitted to the backend of the receiver located in the working building (Fig. 2) through the optical fiber link located in the tunnel. Each backend unit (Fig. 3, bottom-left) processes the signals from four antennas. The input optical signals are converted back to the UHF, amplified, transformed to an intermediate frequency, and digitized at 100 MHz. Their subsequent digital processing includes the formation of the operating frequency band, coarse and fine compensation for the geometric delays and difference in the cable lengths, and fringe stopping. Finally the digital signals come to a correlator mounted in the right cabinet shown in Fig. 3 (bottom right). The correlator currently produces 512 complex visibilities for the imaging and several tens of those for the calibration purposes. Redundant baselines are not used in the imaging.

Single-frequency test observations started at the SRH early in 2016. Since July 2016 till December 2017, the SRH routinely observed the Sun at five frequencies. To monitor solar activity and main SRH systems, the so-called correlation plots are used. Being a proxy of radio flux, they represent temporal variations in the sum of cross-correlations of all antenna pairs (Lesovoi and Kobets, 2017) and show the changes in both the brightness and structure of the sources. Real-time correlation plots and quick-look images produced by the SRH at a set of the operating frequencies are accessible online at the SRH Web site http://badary.iszf.irk.ru/. Adjustment of the SRH systems is still in progress.

Raw SRH data contain complex visibilities measured at a given set of frequencies in right and left circularly-polarized components, information on the array geometry, time stamps, etc. The data are stored in binary FITS tables. The Python-based library providing basic programming user interfaces for data handling, phase calibration, and interferometric imaging routines is under development.